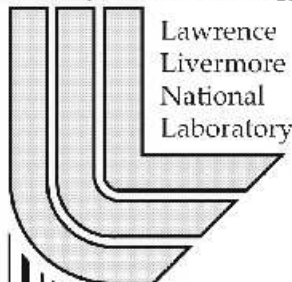


# Robust Background Subtraction With Foreground Validation For Urban Traffic Video

*Sen-ching S. Cheung*  
*Chandrika Kamath*

This article was submitted to EURASIP Journal on Applied  
Signal Processing (Special Issue on Advances in Intelligent  
Vision Systems: Methods and Applications)

U.S. Department of Energy



Lawrence  
Livermore  
National  
Laboratory

**Submitted January 15, 2004**

## **DISCLAIMER**

This document was prepared as an account of work sponsored by an agency of the United States Government. Neither the United States Government nor the University of California nor any of their employees, makes any warranty, express or implied, or assumes any legal liability or responsibility for the accuracy, completeness, or usefulness of any information, apparatus, product, or process disclosed, or represents that its use would not infringe privately owned rights. Reference herein to any specific commercial product, process, or service by trade name, trademark, manufacturer, or otherwise, does not necessarily constitute or imply its endorsement, recommendation, or favoring by the United States Government or the University of California. The views and opinions of authors expressed herein do not necessarily state or reflect those of the United States Government or the University of California, and shall not be used for advertising or product endorsement purposes.

This is a preprint of a paper intended for publication in a journal or proceedings. Since changes may be made before publication, this preprint is made available with the understanding that it will not be cited or reproduced without the permission of the author.

This research was supported under the auspices of the U.S. Department of Energy by the University of California, Lawrence Livermore National Laboratory under contract No. W-7405-Eng-48.

# Robust Background Subtraction With Foreground Validation For Urban Traffic Video

Sen-Ching S. Cheung and Chandrika Kamath

cheung11@llnl.gov, kamath2@llnl.gov  
Center for Applied Scientific Computing  
Lawrence Livermore National Laboratory  
7000 East Avenue, Livermore, CA 94550

## ABSTRACT

Identifying moving objects in a video sequence is a fundamental and critical task in many computer-vision applications. Background subtraction techniques are commonly used to separate foreground moving objects from the background. Most background subtraction techniques assume a single rate of adaptation, which is inadequate for complex scenes such as a traffic intersection where objects are moving at different and varying speeds. In this paper, we propose a foreground validation algorithm that first builds a foreground mask using a slow-adapting Kalman filter, and then validates individual foreground pixels by a simple moving object model, built using both the foreground and background statistics as well as the frame difference. Ground-truth experiments with urban traffic sequences show that our proposed algorithm significantly improves upon results using only Kalman filter or frame-differencing, and outperforms other techniques based on mixture of Gaussians, median filter, and approximated media filter.

**Keywords:** background subtraction, foreground validation, urban traffic video

## 1. INTRODUCTION

Identifying moving objects in a video sequence is a fundamental and critical task in video surveillance, traffic monitoring and analysis, human detection and tracking, and gesture recognition in human-machine interface. A common approach to identifying the moving objects is background subtraction, where each video frame is compared against a reference or background model. Pixels in the current frame that deviate significantly from the background are considered to be moving objects. These “foreground” pixels are further processed for object localization and tracking. Since background subtraction is often the first step in many computer vision applications, it is important that the extracted foreground pixels accurately correspond to the moving objects of interest. Requirements of a good background subtraction algorithm include fast adaptation to changes in environment, robustness in detecting objects moving at different speeds, and low implementation complexity.

At the heart of any background subtraction algorithm is the construction of a statistical model that describes the background state of each pixel. Different algorithms build the background model differently, ranging from a single-state estimate based on median filter [1–5], Weiner filter [6], or Kalman filter [7–12], to a full density estimation based on Gaussian mixture models [13–18] or histograms [19]. All of these algorithms have a fixed design parameter, typically the size of a frame buffer or a recursive update parameter, that determines how adaptive the model is to the change in pixel value. We argue that a fixed parameter is inadequate for scenes such as a traffic intersection where objects move at a variety of speeds. Let us illustrate this with an example.

The top plot in Figure 1(a) shows an example of how a pixel changes its value throughout a period of time. It begins at level 50, then moves to and stays at 150 for a long period of time. A fast-adapting background subtraction algorithm may output its background/foreground decision similar to the middle plot in Figure 1(a): it declares the pixel to be foreground for a short period of time before absorbing the new value as part of the background state. On the other hand, the output decision from a slow-adapting algorithm, shown in the bottom plot in Figure 1(a), stays in foreground for a much longer period.

The issue here is that, depending on the particular situation, either of these algorithms can be wrong. One scenario is shown in the top illustration in Figure 1(b), where an object of gray value 150 is moving slowly to

the right over a background of gray value 50. The resulting foreground masks of a fast-adapting and a slow-adapting algorithms are shown in the middle and bottom illustrations. The slow-adapting algorithm clearly produces better results as the fast-adapting algorithm misses most part of the moving object. The problem of a fast-adapting algorithm failing to detect the motion of a homogeneous object is known as the aperture problem in computer vision [20]. Notice that both algorithms leave a trail of erroneous foreground pixels behind the object as their background models are temporarily corrupted by it. Another possible scenario is shown in Figure 1(c), where an object of gray value 50, stationary at first, starts moving and reveals a background of value 150. The fast-adapting algorithm quickly absorbs the newly-revealed background value and correctly identifies the moving object. The slow-adapting algorithm, however, leaves a ghost impression of the object long after it is gone. These two scenarios demonstrate that a single fixed rate of adaptation is not sufficient for objects moving at different and varying speeds.

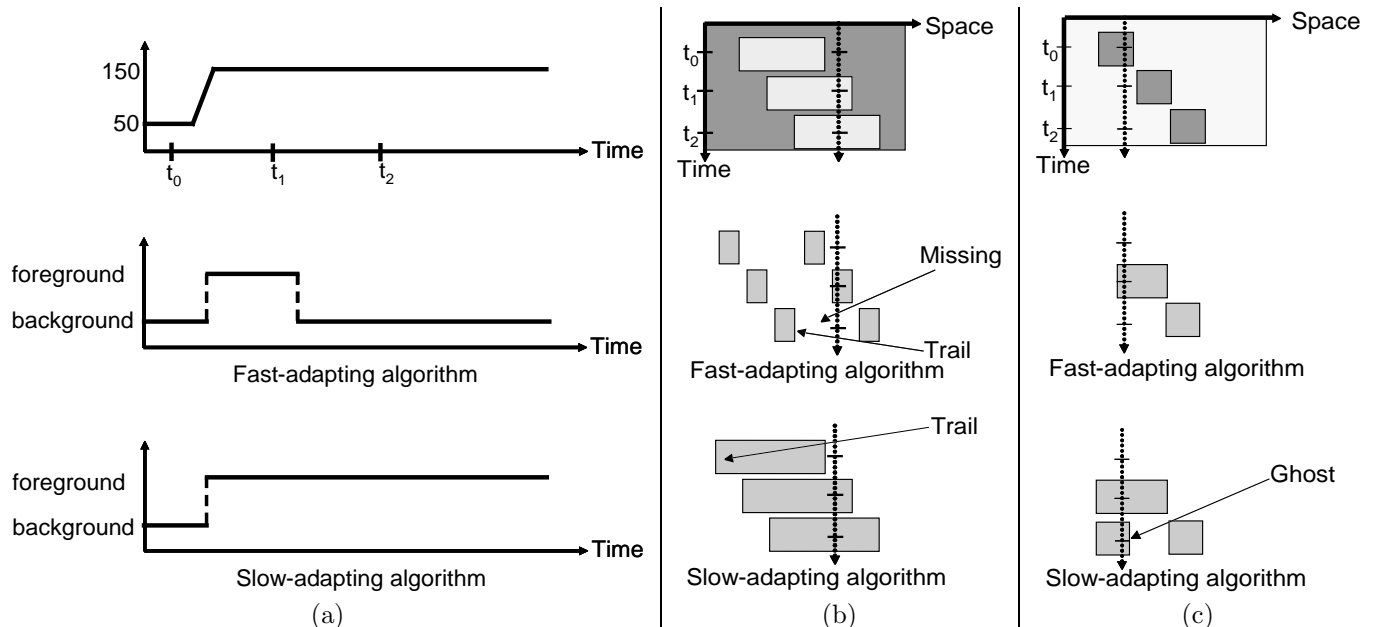


**Figure 1.** The top plot in (a) shows the changes of a pixel over time. The middle and bottom plots in (a) show the foreground/background decisions of a fast-adapting and a slow-adapting background subtraction algorithm respectively. (b) and (c) show two possible scenarios that may correspond to the plots in (a) at time-step  $t_0$ ,  $t_1$ , and  $t_2$ . The top illustration in (b) shows an object moving to the right. The top illustration in (c) shows another object that is stationary at  $t_0$  but starts to move to the right afterwards, revealing the background behind. The middle illustrations show the foreground masks produced by a fast-adapting algorithm for the two scenarios at the same time-steps, and the bottom illustrations show those of a slow-adapting algorithm. The dotted arrows indicate where the pixel values and foreground/background decisions in (a) are sampled at the three time-steps.

The above example also illustrates that it is impossible to determine the correct rate of adaptation by just considering the causal history of a single pixel. In this paper, we propose a novel algorithm that first builds a foreground mask based on a slow-adapting algorithm, and then validates individual foreground pixels by a simple moving object model, built using both the foreground and background statistics as well as a fast-adapting algorithm. Our primary focus is on detecting moving vehicles and pedestrians in video sequences of urban traffic. This paper is organized as follows: we describe the proposed algorithm in Section 2 and contrast it with related work in Section 3. We apply our proposed algorithm and other background subtraction techniques on a set of urban traffic video sequences. Results of subjective evaluations and objective performance measurements with respect to a ground-truth are presented in Section 4. In Section 5, we conclude the paper by discussing limitations of our algorithm and possible future work.

## 2. PROPOSED ALGORITHM

This section describes our proposed algorithm for validating a foreground mask computed by a slow-adapting background subtraction algorithm. Figure 2 shows the schematic diagram of our algorithm. The output is a binary foreground mask  $F_t$  at time  $t$  with  $F_t(\mathbf{p}) = 1$  indicating a foreground pixel detected at location  $\mathbf{p}$ . There are three inputs to the algorithm: 1)  $I_t$  is the video frame at time  $t$ ; 2)  $P_t$  is the binary foreground mask from a slow-adapting background subtraction algorithm; 3)  $D_t$  denotes the foreground mask obtained by thresholding on the normal statistics of the difference between  $I_t$  and  $I_{t-1}$ , i.e.  $D_t(\mathbf{p}) = 1$  if

$$\frac{|I_t(\mathbf{p}) - I_{t-1}(\mathbf{p}) - \mu_d|}{\sigma_d} > T_d, \quad (1)$$

and zero otherwise.  $\mu_d$  and  $\sigma_d$  are the mean and the standard deviation of  $I_t(\mathbf{q}) - I_{t-1}(\mathbf{q})$  for all spatial locations  $\mathbf{q}$ . Frame-differencing is the ultimate fast-adapting background subtraction algorithm. Even though it suffers from severe aperture problem, we choose frame-differencing because it leaves only a short foreground trail behind a moving object as its memory does not extend beyond the previous frame. There are five components in our algorithm: blob formation, core object identification, object histogram, background histogram, and object extension. Their functions are explained below.

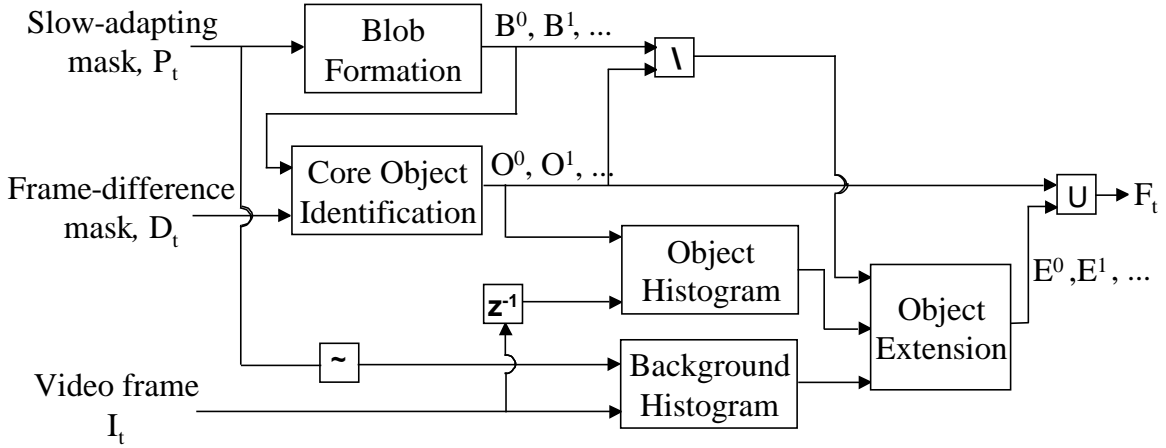


**Figure 2.** Structure of the data validation module.

In blob formation, all the foreground pixels in  $P_t$  are grouped into disconnected blobs  $B^0, B^1, \dots, B^N$  based on the assumption that each foreground pixel is connected to all of its eight adjacent foreground pixels [20]. A blob may contain 1) no object, 2) part of a moving object, 3) a single moving object with possible foreground trail, and 4) multiple moving objects. The first case corresponds to the foreground ghost as explained in Section 1. The second case is likely the result of the aperture problem. Since  $P_t$  is computed by a slow-adapting algorithm, the aperture problem occurs only when an object is starting to move. Most blobs fall into the third case of a single object. The last case of multiple objects occur when multiple vehicles start moving after a traffic light has turned green. We ignore the last case as the large blob is likely to break down into multiple single-object blobs once the traffic disperses. The main goals of our algorithm are 1) to eliminate all the ghost blobs, 2) to maintain the partial-object blobs so that they can grow to contain the full objects, and 3) to produce better localization for single-object blobs by removing any foreground trail. We accomplish these goals by validating each blob with the frame-difference mask  $D_t$  in the core object identification module.

The core object identification module first eliminates all the blobs that do not contain any foreground pixels from  $D_t$ . This step removes all the ghost blobs which produce no significant frame differences as there are no moving objects in them. The module then computes a core object  $O^i$  for each of the remaining blobs  $B^i$ .  $O^i$  is defined as follows:

$$O^i = \text{Bounding\_Ellipse}\{\mathbf{p} : \mathbf{p} \in B^i \text{ and } D_t(\mathbf{p}) = 1\} \cap B^i. \quad (2)$$

We illustrate our definition of  $O^i$  using a single moving object as shown in Figure 3(a). The blob contains both the object and its foreground trail. The frame-difference mask  $D_t$  captures the front part of the object and the small area trailing the object, but completely ignores the rest of the foreground trail of the blob. Taking advantage of the shape of a typical vehicle, we assume that the object is contained within the bounding ellipse of all the foreground pixels from  $D_t$  inside the blob. The key idea is that we can use the bounding ellipse to exclude most of the foreground trail from the blob. The bounding ellipse is computed by first calculating its two foci and orientation based on the first and second-order moments of the foreground pixels in  $D_t$  [21], and then increasing the length of its major axis until it contains all the foreground pixels. Finally, we output the intersection between the bounding ellipse and the blob shown in Figure 3(b) as the core object  $O^i$ .

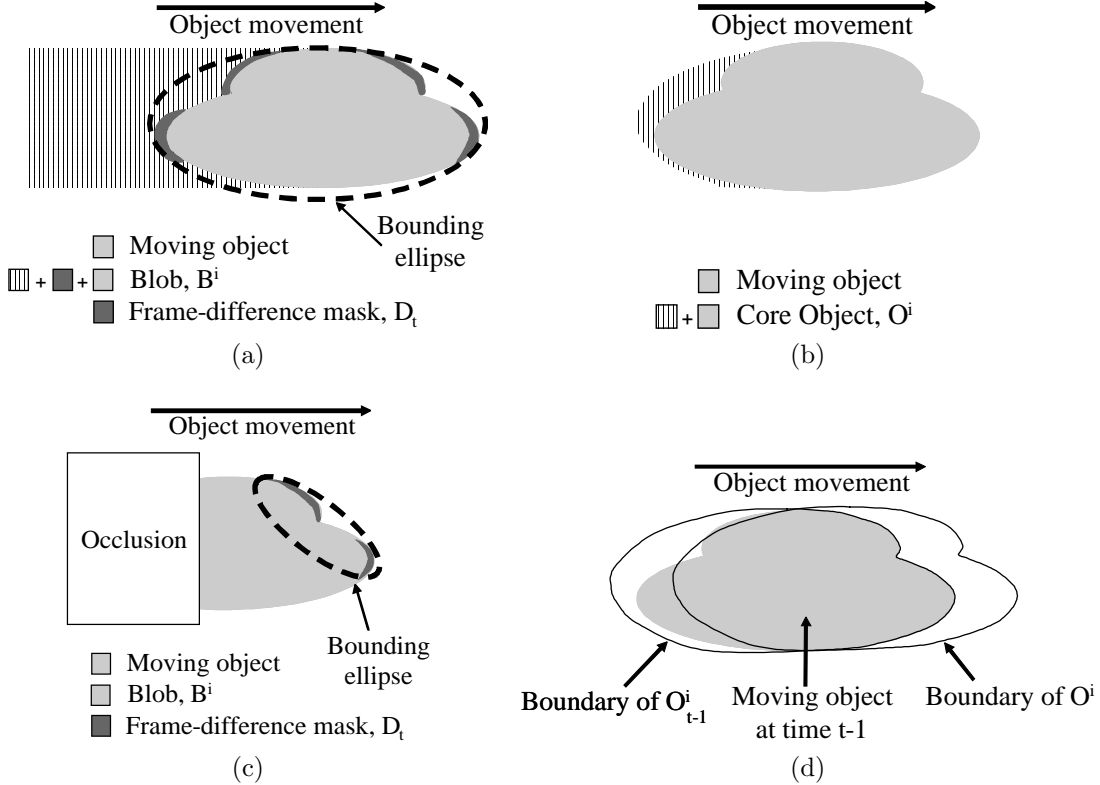


**Figure 3.** (a) The bounding ellipse is defined by the frame-difference foreground pixels within the blob; (b) The intersection of the bounding ellipse and the blob identifies the core object  $O^i$ ; (c) The bounding ellipse may fail to include the full object emerging from occlusion; (d) The intersection of the core objects at time  $t - 1$  and  $t$  is used for estimating the object histogram.

Our experience with urban traffic sequences indicates that most moving objects can be adequately represented by their corresponding core objects. Nevertheless, there are situations where the core object captures only a small portion of the entire moving object. Consider the example of a vehicle emerging from an occlusion as shown in Figure 3(c). Even though the blob may contain the entire moving object, the foreground pixels from  $D_t$  are present only in the front, resulting in a small core object  $O^i$  covering that part of the object. The object extension module in Figure 2 is responsible to thrust back some of the blob pixels outside  $O^i$  back into foreground. For every pixel  $\mathbf{p}$  in  $B^i$  outside  $O^i$ , the object extension module declares  $\mathbf{p}$  to be foreground if  $\mathbf{p}$  is more likely to be part of the core object  $O^i$  than part of the background. The module thus needs to estimate the Probability Density Functions (PDF) of both the background and the object.

To estimate the background PDF, we first partition the current video frame into  $M$  rectangular regions  $R_1, R_2, \dots, R_M$ . Then, for each region  $R_j$ , we compute a background histogram  $h_j$  for all the pixels in  $R_j$  that

are not part of  $P_t$ , i.e.

$$h_j(s) = \frac{|\{\mathbf{p} : \mathbf{p} \in R_j \text{ and } P_t(\mathbf{p}) = 1 \text{ and } I_t(\mathbf{p}) = s\}|}{|\{\mathbf{p} : \mathbf{p} \in R_j \text{ and } P_t(\mathbf{p}) = 1\}|}, \quad (3)$$

for  $j = 1, 2, \dots, M$ . In our implementation, we partition  $I_t$  into  $M = 64$  identical rectangular regions.

To build the object histogram, we notice from Figure 3(b) that the core object  $O^i$ , as defined in Equation (2), may contain pixels that are not part of the object. It is shown in [6] that the only pixels guaranteed to be part of the object are pixels from  $I_{t-1}$  that are foreground in both  $D_t$  and  $D_{t-1}$ . Based on our experience, this approach does not always produce sufficient number of pixels to reliably estimate the object histogram. Instead, for each core object  $O^i$ , we first identify the corresponding core object at time  $t-1$ , which we denote as  $O_{t-1}^i$ . We accomplish this by finding the core object at time  $t-1$  that has the biggest overlap with  $O^i$ . Then, we compute the intersection between  $O^i$  and  $O_{t-1}^i$  and build the histogram of the pixels from  $I_{t-1}$  under this intersection. This procedure is illustrated in Figure 3(d). The object histogram  $g_i$  for core object  $O^i$  can now be defined as follows:

$$g_i(s) = \frac{|\{\mathbf{p} : \mathbf{p} \in O^i \cap O_{t-1}^i \text{ and } I_{t-1}(\mathbf{p}) = s\}|}{|\{\mathbf{p} : \mathbf{p} \in O^i \cap O_{t-1}^i\}|}. \quad (4)$$

Combining the histograms from (3) and (4), the object extension module defines the object extension  $E^i$  as follows:

$$E^i = \{\mathbf{p} : \mathbf{p} \in B^i \setminus O^i \text{ and } g_i(I_t(\mathbf{p})) \geq h_j(I_t(\mathbf{p})) \text{ with } \mathbf{p} \in R_j\} \quad (5)$$

The final output mask  $F^t$  is simply the union of all the core objects  $O^i$  and the object extensions  $E^i$ .

### 3. RELATED WORK

In this section, we review related work in background modelling and foreground validation. We first summarize some of the representative schemes for background modelling. A more detailed exposition can be found in [22]. We classify background modelling algorithms into non-recursive and recursive techniques. A non-recursive technique maintains a buffer of video frames and uses a sliding-window approach for background estimation. In order to keep a long history with low storage requirement, video frames can be stored into the buffer at a frame-rate  $r$  lower than the input rate. The most commonly-used non-recursive technique is median filtering [1–5]. The background estimate is defined to be the median at each pixel location of all the frames in the buffer. Wiener filter is used in [6], where the filter coefficients are estimated at each frame time based on the sample covariances. Unlike median filter or Wiener filter which produce a single background estimate, Elgammal et al. [19] build a background PDF using a Gaussian kernel estimator. The advantage of using a full density function over a single estimate is the ability to handle multi-modal background distribution. Examples of multi-modal background include pixels from moving leaves of a swinging tree or pixels near high-contrast edges which flicker under small camera movement.

Recursive techniques recursively update a single background model and do not store a buffer of video frames. The two simplest recursive techniques are approximated median filter [23, 24] and Kalman filter [7–12]. Approximated median filter increments a running estimate of the median by one if the input pixel is larger than the estimate, and decrements by one if smaller. Kalman filter is a widely-used recursive technique for tracking linear dynamical systems under Gaussian noise. Many different versions have been proposed for background modelling, differed mainly in the state spaces they use for tracking. We provide a brief description of the popular scheme used in [7]: the internal state at pixel location  $\mathbf{p}$  of the Kalman Filter is described by the background intensity  $S_t(\mathbf{p})$  and its temporal derivative  $S'_t(\mathbf{p})$ , which are recursively updated as follows:

$$\begin{bmatrix} S_t(\mathbf{p}) \\ S'_t(\mathbf{p}) \end{bmatrix} = \mathbf{A} \cdot \begin{bmatrix} S_{t-1}(\mathbf{p}) \\ S'_{t-1}(\mathbf{p}) \end{bmatrix} + \mathbf{K} \cdot \left( I_t(\mathbf{p}) - \mathbf{H} \cdot \mathbf{A} \cdot \begin{bmatrix} S_{t-1}(\mathbf{p}) \\ S'_{t-1}(\mathbf{p}) \end{bmatrix} \right) \quad (6)$$

Matrix  $\mathbf{A}$  describes the background dynamics and  $\mathbf{H}$  is the measurement matrix. The Kalman gain matrix  $\mathbf{K}$  switches between a slow adaptation rate  $\alpha_1$  and a fast adaptation rate  $\alpha_2 > \alpha_1$  based on the feedback of the foreground mask  $F_{t-1}$ :

$$\mathbf{K} = \begin{bmatrix} \alpha_1 \\ \alpha_1 \end{bmatrix} \text{ if } F_{t-1}(\mathbf{p}) = 1, \text{ and } \begin{bmatrix} \alpha_2 \\ \alpha_2 \end{bmatrix} \text{ otherwise.} \quad (7)$$

Another popular recursive technique is the Mixture of Gaussian (MoG), which tracks the background distribution as a linear sum of  $K$  Gaussian component densities [13–18]. If the new input pixel  $I_t(\mathbf{p})$  is close to one of the Gaussian component, the mean and the standard deviation of that component is updated. Otherwise, the least probable one is deleted and a new component is added centered at  $I_t(\mathbf{p})$  [14]. The weights of all the components are decayed at a rate of  $(1 - \alpha)$ , except for the weight of the updated component which is incremented by  $\alpha$ . To determine which components correspond to the background, all components are first ranked by the ratios between their weights and standard deviations. Then, the first  $N$  components that satisfy the following criterion are declared to be the background components:

$$\sum_{k=i_1}^{i_N} \omega_{k,t} \geq \Gamma, \quad (8)$$

where  $\omega_{k,i_1}, \dots, \omega_{k,i_N}$  are the weights of the components after ranking, and  $\Gamma > 0$  is the weight threshold.  $I_t$  is declared as background if it is within  $D$  times the standard deviation from the mean of any one of the background components.

Many foreground validation techniques have also been proposed in the literature. Some of them incorporate knowledge from the high-level applications such as tracking [9, 25], or use extra information such as depth [25, 26] to improve the background model. Optical flow is also commonly used to detect ghost blobs [5, 27]. In contrast to these approaches, our algorithm does not rely on any external information and uses the much simpler frame-differencing for ghost-blob removal. Algorithms have also been proposed to combine multiple background models running at different adaptation rates [12, 19]. However, the combination is done by a simple conjunction at the pixel level, rather than at the blob level as in our algorithm. Pixel-level combination might lead to the aperture problem as the fast-adapting algorithm can fail to detect slow-moving objects. Blob-level processing has been proposed in [6] for foreground validation. Similar to our algorithm, [6] builds core objects based on the intersection of a slow-adapting mask and the frame-difference mask, and grows the core objects using object histograms and connected component grouping. Nevertheless, lackluster results are reported in [6] because, by growing the core objects from a waving tree, the blob-level processing turns part of the sky into foreground. There are three key differences between our proposed algorithm and that proposed in [6]. First, in our proposed algorithm, the object growing is confined within the slow-adapting mask, thus limiting the amount of false-positives the algorithm can introduce. Second, we use both the object histogram and the background histogram to achieve reliable object growing. Finally, using a bounding ellipse as a first order approximation to the object leads to a significant speedup as it already accounts for most of the foreground pixels.

#### 4. EXPERIMENTAL RESULTS

In this section, we compare the performance of our proposed algorithm with other algorithms in the literature. We apply the background subtraction algorithms to luminance sequences only. For preprocessing, we first apply a three-frame temporal erosion to the test sequence, that is we replace  $I_t$  with the minimum of  $I_{t-1}$ ,  $I_t$ , and  $I_{t+1}$ . This step can reduce temporal camera noise and mitigate the effect of snowfall present in one of our test sequences. Then, a  $3 \times 3$  spatial Gaussian filter is used to reduce spatial camera noise.

Even though our proposed algorithm can work with any slow-adapting background subtraction algorithm, we have chosen Kalman filter as described in Section 3 for its simplicity in implementation. To propagate the validation results to future frames, we use the output mask  $F_t$  from the foreground validation for feedback in the Kalman filter. The parameters of the Kalman filter are set as follows [7]:

$$\mathbf{A} = \begin{bmatrix} 1 & 0.7 \\ 0 & 0.7 \end{bmatrix}, \quad \mathbf{H} = [1 \ 0], \quad \alpha_1 = 0.001, \quad \alpha_2 = 0.05. \quad (9)$$

Similar to the frame-difference thresholding in Equation (1),  $P_t(\mathbf{p}) = 1$  if

$$\frac{|I_t(\mathbf{p}) - S_t(\mathbf{p}) - \mu_k|}{\sigma_k} > T_k, \quad (10)$$



where  $S_t(\mathbf{p})$  is the internal state of the Kalman filter, and  $\mu_k$  and  $\sigma_k$  are the mean and the standard deviation of  $I_t(\mathbf{q}) - S_t(\mathbf{q})$  for all spatial locations  $\mathbf{q}$  in the frame. In our experiments, we set the frame-difference foreground threshold  $T_d$  to be 2.0, and vary the Kalman filter foreground threshold  $T_k$  to show the trade-off between false-positives and false-negatives in foreground detection.

The set of algorithms used for comparison include frame differencing (FD), approximated median filter (AMF), Kalman filter without validation (KF), median filter (MF), and Mixture of Gaussian (MoG). Based on our earlier work in [22], we have selected particular values for the parameters in these algorithms that perform well in our test sequences. These fixed parameters are listed in Table 1. The most sensitive parameter in each algorithm is used as the test parameter to show the trade-off between false-positives and false-negatives.

Schemes	Fixed parameters	Test parameter
Frame differencing (FD)	None	Foreground threshold $T_d$
Approximated median filter (AMF)	None	Foreground threshold $T$
Kalman filter (KF)	$\alpha_1 = 0.001, \alpha_2 = 0.05$	Foreground threshold $T_k$
Median filter (MF)	Buffer size $L = 9$ Buffer sampling rate $r = 10$ frame/sec	Foreground threshold $T$
Mixture of Gaussian (MoG)	Number of components $K = 3$ Adaptation rate $\alpha = 0.05$ Weight threshold $\Gamma = 0.25$ Initial variance $\sigma_o^2 = 36$ Initial weight $\omega_o = 0.1$	Deviation threshold $D$

**Table 1.** Background modelling schemes and their parameters.

#### 4.1. Test Sequences

We have selected four publicly-available urban traffic video sequences from the website maintained by KOGS/-IAKS Universitaet Karlsruhe\*. A sample frame from each sequence is shown in the first row of Figure 4. The first sequence is called “Bright”, which is 1500 frames long showing a traffic intersection in bright daylight. The second sequence is called “Fog”, which is 300 frames long showing the same traffic intersection in heavy fog. The third sequence “Snow” is also 300 frames long and shows the intersection while snowing. Fog and Snow were originally in color; we have first converted them into luminance and discarded the chroma channels. The first three sequences all have low to moderate traffic, and contain “stop-and-go” traffic – vehicles come to a stop in front of a red-light and start moving once the light turns green.. The last sequence “Busy” is 300 frames long. It shows a busy intersection with the majority of the vehicle traffic flowing from the top left corner to the right side.

#### 4.2. Evaluation

In order to have a quantitative evaluation of the performance, we have selected ten frames at regular intervals from each test sequence, and manually highlighted all the moving objects in them. These “ground-truth” frames are selected from the latter part of each of the test sequences<sup>†</sup> to minimize the effect of the initial adaptation of the algorithms. In the manual annotation, we highlight only the pixels belonging to vehicles and pedestrians that are actually moving at that frame. Since we do not use any shadow suppression scheme in our comparison, we also include those shadow pixels cast by moving objects. The ground-truth frames showing only the moving objects are shown in the second row of Figure 4.

\*The URL is [http://i21www.ira.uka.de/image\\_sequences](http://i21www.ira.uka.de/image_sequences). All sequences are copyrighted by H.-H. Nagel of KOGS/IAKS Universitaet Karlsruhe.

<sup>†</sup>The ground-truth frames are selected from the last 1000 frames in the Bright sequence, and the last 200 frames in the remaining three sequences.

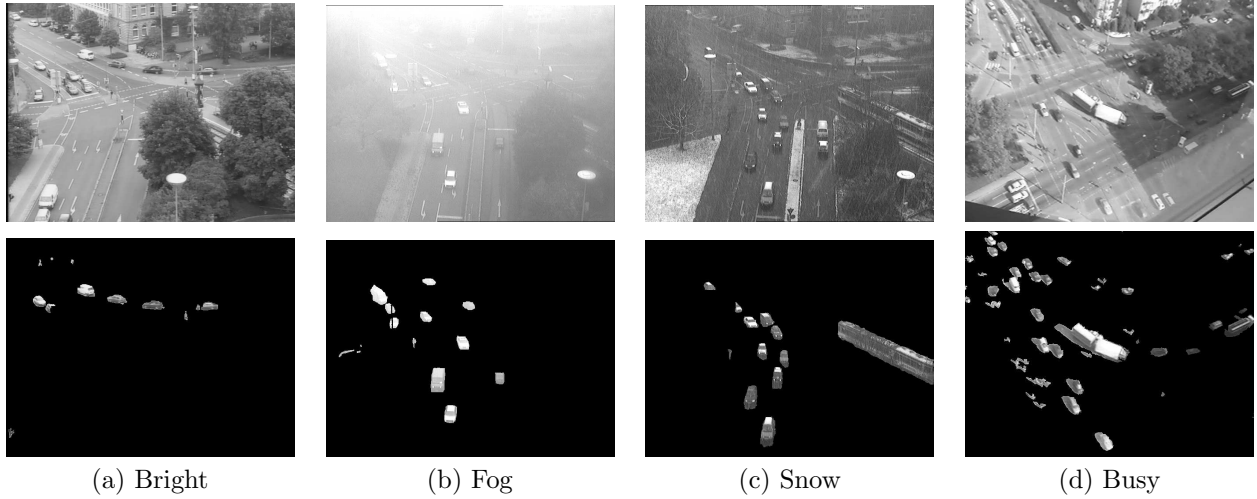


**Figure 4.** Sample frames and the corresponding ground-truth frames from the four test sequences: *Bright*, *Fog*, *Snow*, and *Busy*.

We use two information retrieval measurements, recall and precision, to quantify how well each algorithm matches the ground-truth [28]. They are defined in our context as follows:

$$\text{Recall} = \frac{\text{Number of foreground pixels correctly identified by the algorithm}}{\text{Number of foreground pixels in ground-truth}} \quad (11)$$

$$\text{Precision} = \frac{\text{Number of foreground pixels correctly identified by the algorithm}}{\text{Number of foreground pixels detected by the algorithm}} \quad (12)$$

Recall and precision values are both within the range of 0 and 1. When applied to the entire sequence, the recall and precision reported are averages over all the measured frames. Typically, there is a trade-off between recall and precision – recall usually increases with the number of foreground pixels detected, which in turn may lead to a decrease in precision. A good background algorithm should attain as high a recall value as possible without sacrificing precision.

By varying the testing parameter of each algorithm, we obtain the Precision-Recall (PR) curves for the test sequences as shown in Figure 5(a) to (d). Notice that the PR curves of all the non-recursive techniques (FD, AMF, MF) are almost continuous over the entire range of recall values, while those from the recursive ones (MoG, KF, Proposed) are discrete, occupying shorter ranges of recall. The reason is that non-recursive techniques do not have a feedback loop so that it is possible to run the simulation once and compute the precision and the recall for any test parameter value. Recursive techniques require a separate simulation for each different test parameter value, and thus we only obtain results at a few operating points.

Figure 5(a) shows the results of the sequence “Bright”. The worst performer is FD and the best performer, at least for recall above 60%, is our proposed algorithm. Our proposed algorithm shares a similar shape with KF but has a much better precision. MoG outperforms the proposed algorithm at low recall primarily because MoG can adapt its threshold for each pixel individually, while our proposed algorithm relies on the global standard deviation. As some of the ground-truth frames have only a few moving objects, the global standard deviation becomes quite small. This turns some of the background pixels into foreground erroneously and thus lowers the precision values. The PR curves of “Fog” in Figure 5(b) follow a similar trend as those in Figure 5(a).

Figure 5(c) shows that our proposed algorithm significantly outperforms all the other schemes in the sequence “Snow”. This can be explained by the two thresholds  $T_d$  and  $T_k$  used in our proposed algorithm. The “Snow” sequence is very noisy and all other algorithms need high foreground thresholds to prevent excessive false foreground, thus resulting in low recall values. On the other hand, our proposed algorithm can use a small threshold  $T_k$  in the Kalman filter to get good coverage of the moving objects, but uses a large frame-difference threshold  $T_d$  for building the correct shapes of the objects and removing the ghost foreground blobs.

In the final sequence “Busy”, our proposed algorithm performs worse than MoG and MF for recall values above 60%. This reversal of performance is due to the large number of moving objects clustered together in “Busy”. At high recall values, the foreground threshold of the Kalman filter is small, creating a large blob that contains many moving objects. The resulting bounding ellipse is not able to eliminate any of the false foreground between vehicles, leading to a low precision value.

We further illustrate the differences between the algorithms using two sets of extracted foreground images in Figure 6 and 7. The corresponding original images are shown in Figure 8. Figure 6 is extracted from “Bright”, showing a car moving to the left and a pedestrian walking to the right. FD is noisy and captures only fragments of the car due to the aperture problem. Both AMF and KF leave a foreground trail behind each moving object as their background states are corrupted. MF, MoG, and the proposed algorithm produce similar results. Figure 7 is extracted from “Snow” showing a car starting to move to the bottom after being stationary for a long time. AMF, KF, and MF leave a ghost foreground behind the moving car. MoG is less problematic but still has much noise. FD and the proposed algorithm have no ghost at all. Only the proposed algorithm produces an almost-perfect localization of the car. Notice that even the low-contrast windshield is captured due to the two thresholds used in the proposed algorithm as explained earlier.

## 5. CONCLUSIONS

In this paper, we have introduced a new algorithm to validate foreground regions or blobs captured by a slow-adapting background subtraction algorithm. By comparing the blobs with bounding ellipses formed by frame-difference foreground pixels, the algorithm can eliminate false foreground trails and ghost blobs that do not contain any moving object. Better object localization under occlusion is accomplished by extending the ellipses using the object and background pixel distributions. Ground-truth experiments with urban traffic sequences have shown that our proposed algorithm produces performance that are comparable or better than other background subtraction techniques.

Our proposed algorithm, however, has a number of limitations. First, the use of bounding ellipses may not be appropriate for complex-shaped objects such as human beings. Second, we use frame-differencing as it produces minimal false foreground trails behind objects. This assumption may not hold if the input video frame rate is very low. Finally, as described in Section 4.2, the proposed algorithm does not perform well when there are multiple moving objects close to each other. We are currently improving our algorithm by building multiple ellipses to identify moving objects and using the background distribution to identify the background area among them.

## ACKNOWLEDGMENTS

UCRL-JC-xxxxxxx: This work was performed under the auspices of the U.S. Department of Energy by University of California Lawrence Livermore National Laboratory under contract No. W-7405-Eng-48.

## REFERENCES

1. B. Gloyer, H. Aghajan, K.-Y. Siu, and T. Kailath, “Video-based freeway monitoring system using recursive vehicle tracking,” in *Proceedings of SPIE*, **2421**, pp. 173–180, Feb 1995.
2. R. Cutler and L. Davis, “View-based detection,” in *Proceedings Fourteenth International Conference on Pattern Recognition*, **1**, pp. 495–500, (Brisbane, Australia), Aug 1998.
3. B. Lo and S. Velastin, “Automatic congestion detection system for underground platforms,” in *Proceedings of 2001 International symposium on intelligent multimedia, video, and speech processing*, pp. 158–161, (Hong Kong), May 2001.
4. Q. Zhou and J. Aggarwal, “Tracking and classifying moving objects from videos,” in *Proceedings of IEEE Workshop on Performance Evaluation of Tracking and Surveillance*, 2001.
5. R. Cucchiara, M. Piccardi, and A. Prati, “Detecting moving objects, ghosts, and shadows in video streams,” *IEEE Transactions on Pattern Analysis and Machine Intelligence* **25**, pp. 1337–1342, Oct 2003.
6. K. Toyama, J. Krumm, B. Brumitt, and B. Meyers, “Wallflower: Principles and practice of background maintenance,” in *ICCV (1)*, pp. 255–261, 1999.

7. K.-P. Karmann and A. Brandt, "Moving object recognition using an adaptive background memory," in *Time-Varying Image Processing and Moving Object Recognition*, V. Cappellini, ed., **2**, pp. 289–307, Elsevier Science Publishers B.V., 1990.
8. D. Koller, J. Weber, and J. Malik, "Robust multiple car tracking with occlusion reasoning," Tech. Rep. UCB/CSD-93-780, EECS Department, University of California, Berkeley, Oct 1993.
9. C. Wren, A. Azabajejani, T. Darrel, and A. Pentland, "Pfinder: Real-time tracking of the human body," *IEEE Transactions on Pattern Analysis and Machine Intelligence* **19**, pp. 780–785, July 1997.
10. J. Heikkila and O. Silven, "A real-time system for monitoring of cyclists and pedestrians," in *Second IEEE Workshop on Visual Surveillance*, pp. 246–252, (Fort Collins, Colorado), Jun 1999.
11. G. Halevy and D. Weinshall, "Motion of disturbances: detection and tracking of multi-body non-rigid motion," *Maching Vision and Applications* **11**, pp. 122–137, 1999.
12. T. Boulton *et al.*, "Frame-rate omnidirectional surveillance and tracking of camouflaged and occluded targets," in *Proceedings Second IEEE Workshop on Visual Surveillance*, pp. 48–55, (Fort Collins, CO), June 1999.
13. N. Friedman and S. Russell, "Image segmentation in video sequences: A probabilistic approach," in *Proceedings of the Thirteenth Annual Conference on Uncertainty in Artificial Intelligence (UAI-97)*, pp. 175–181, Morgan Kaufmann Publishers, Inc., (San Francisco, CA), 1997.
14. C. Stauffer and W. Grimson, "Learning patterns of activity using real-time tracking," in *IEEE Trans. on Pattern Analysis and Machine Intelligence*, **22**, pp. 747–57, Aug 2000.
15. X. Gao, T. Boulton, F. Coetzee, and V. Ramesh, "Error analysis of background adaption," in *Proceedings IEEE conference on computer vision and pattern recognition*, **1**, pp. 503–510, (Hilton Head Island, SC), June 2000.
16. P. KaewTraKulPong and R. Bowden, "An improved adaptive background mixture model for real-time tracking with shadow detection," in *Proceedings of the 2nd European Workshop on Advanced Video-Based Surveillance Systems*, Sept. 2001.
17. P. W. Power and J. A. Schoonees, "Understanding background mixture models for foreground segmentation," in *Proceedings Image and Vision Computing New Zealand*, pp. 267–271, (Auckland, New Zealand), Nov 2002.
18. D.-S. Lee, J. Hull, and B. Erol, "A Bayesian framework for gaussian mixture background modeling," in *Proceedings of IEEE International Conference on Image Processing*, (Barcelona, Spain), Sept 2003.
19. A. Elgammal, D. Harwood, and L. Davis, "Non-parametric model for background subtraction," in *Proceedings of IEEE ICCV'99 Frame-rate workshop*, Sept 1999.
20. D. H. Ballard and C. M. Brown, *Computer Vision*, Prentice-Hall, Inc., Englewood Cliffs, NJ, 1982.
21. R. Mukundan and K. R. Ramakrishnam, *Moment Functions in Image Analysis*, World Scientific, 1998.
22. S.-C. Cheung and C. Kamath, "Robust techniques for background subtraction in urban traff," in *Proceedings of Video Communications and Image Processing, SPIE Electronic Imaging*, Jan 2004.
23. N. McFarlane and C. Schofield, "Segmentation and tracking of piglets in images," *Machine Vision and Applications* **8**(3), pp. 187–193, 1995.
24. P. Remagnino *et al.*, "An integrated traffic and pedestrian model-based vision system," in *Proceedings of the Eighth British Machine Vision Conference*, pp. 380–389, 1997.
25. M. Harville, "A framework for high-level feedback to adaptive, per-pixel, mixture-of-Gaussian background models," in *Proceedings of the Seventh European Conference on Computer Vision, Part III*, pp. 543–60, (Copenhagen, Denmark), May 2002.
26. Y. Ivanov, A. Bobick, and J. Liu, "Fast lighting independent background," *International Journal of Computer Vision* **37**(2), pp. 199–207, 2000.
27. D. Gutchess *et al.*, "A background model initialization algorithm for video surveillance," in *Proceedings Eighth IEEE International Conference on Computer Vision*, **1**, pp. 744–740, (Vancouver, BC), July 2001.
28. C. J. van Rijsbergen, *Information retrieval*, Butterworth & Co (Publishers) Ltd, second ed., 1979.

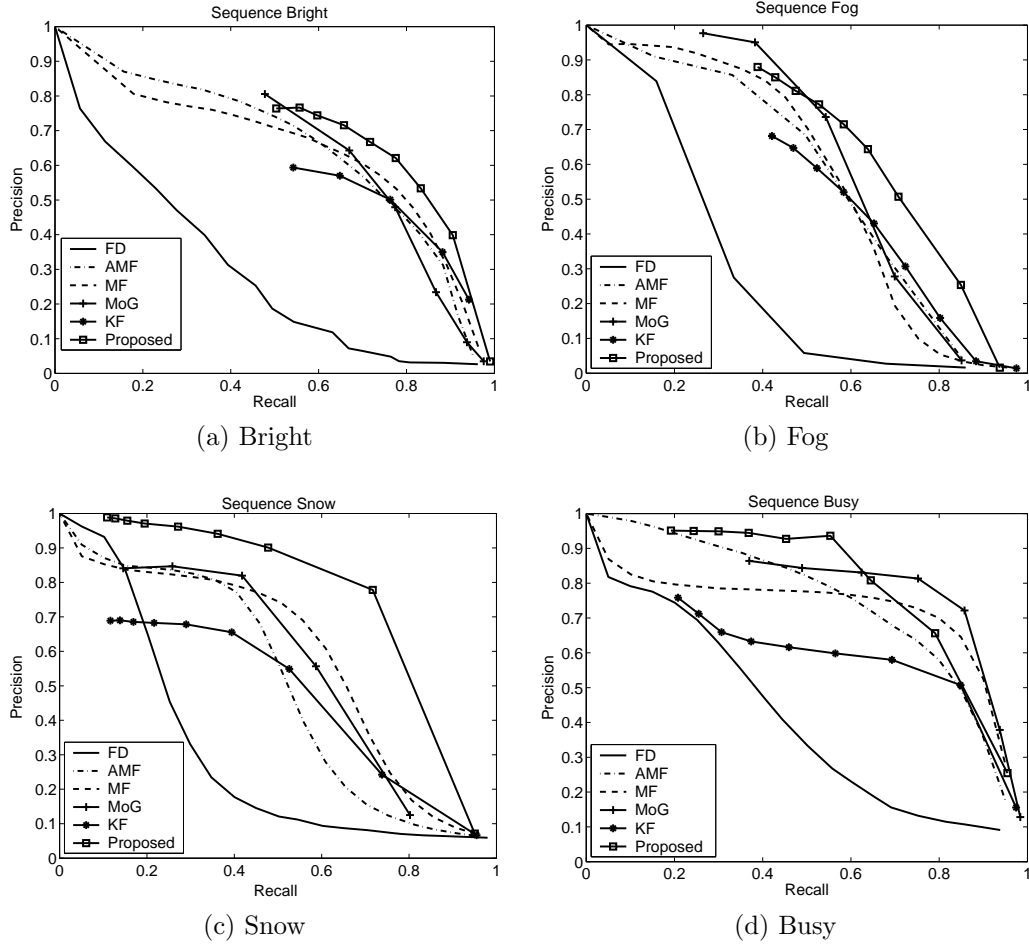


**Figure 5.** Precision-recall plots for (a) Bright, (b) Fog, (c) Snow, and (d) Busy.

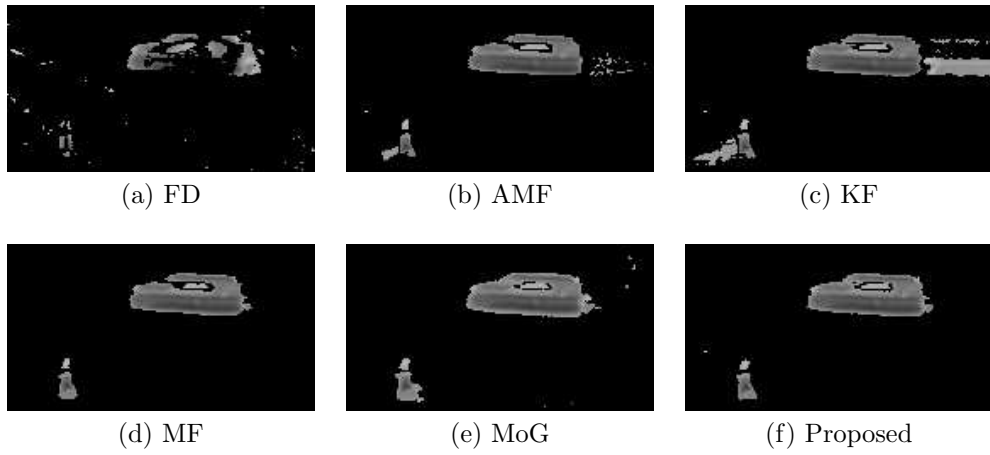


**Figure 6.** Foreground images identified by various algorithms showing a moving car and a pedestrian in sequence "Bright".

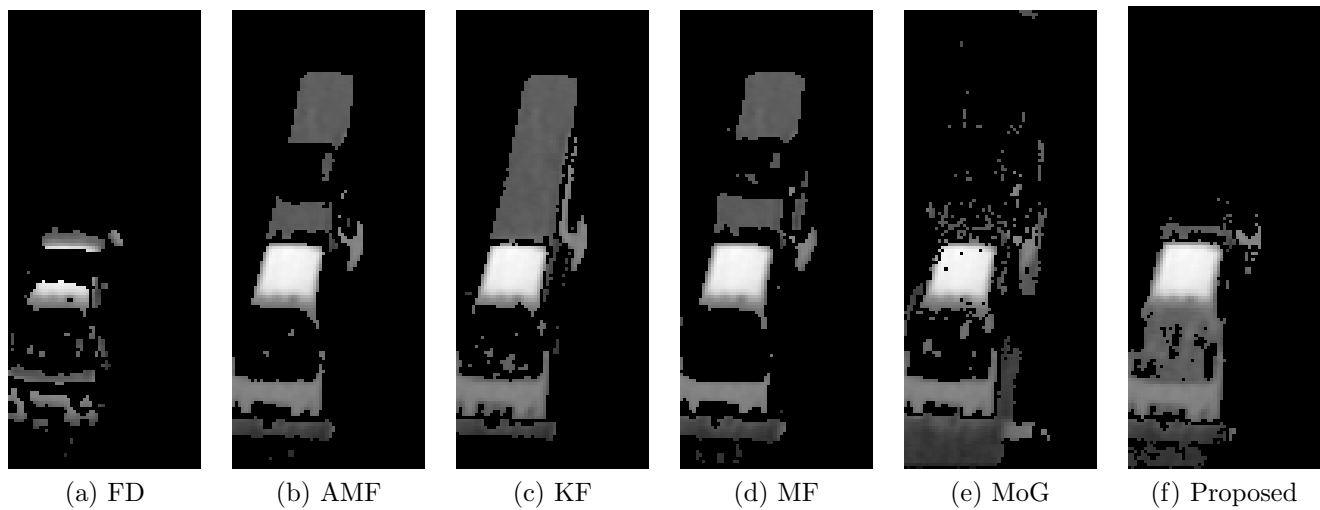


**Figure 7.** *Foreground images identified by various algorithms showing a car that starts to move after being stationary for awhile in sequence “Snow”.*

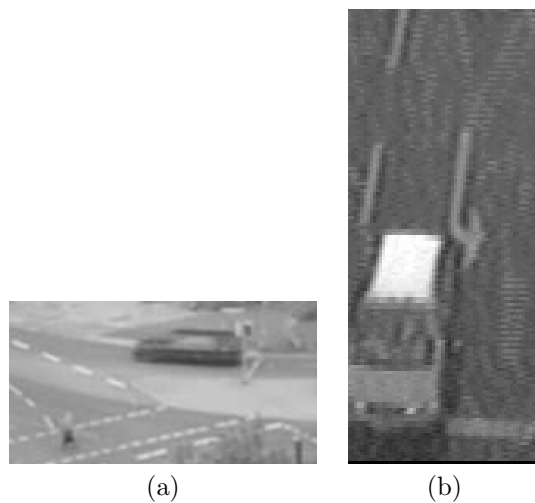


**Figure 8.** *(a) and (b) show the original images corresponding to the foreground masks in Figure 6 and 7.*